

Accelerating design optimization using reduced order models

Youngsoo Choi*, Geoffrey Oxberry, Daniel White, Trenton Kirchdoerfer

Lawrence Livermore National Laboratory †

Abstract

Although design optimization has shown its great power of automatizing the whole design process and providing an optimal design, using sophisticated computational models, its process can be formidable due to a computationally expensive large-scale linear system of equations to solve, associated with underlying physics models. We introduce a general reduced order model-based design optimization acceleration approach that is applicable not only to design optimization problems, but also to any PDE-constrained optimization problems. The acceleration is achieved by two techniques: i) *allowing an inexact linear solve* and ii) *reducing the number of iterations in Krylov subspace iterative methods*. The choice between two techniques are made, based on how close a current design point to an optimal point. The advantage of the acceleration approach is demonstrated in topology optimization examples, including both compliance minimization and stress-constrained problems, where it achieves a tremendous reduction and speed-up when a traditional preconditioner fails to achieve a considerable reduction in the number of linear solve iterations.

Keywords— design optimization, reduced order models, incremental SVD, KKT conditions, Krylov subspace iterative method, topology optimization, compliance minimization, stress-constrained problem

1 Introduction

Design optimization is a powerful tool that enables an automatic process of obtaining an optimal design with the help of sophisticated computational models. It is widely used in industries, academia, laboratories for various applications, mainly including aerospace, structural, mechanical, and biomedical engineering. Many researchers also try to expand its physics domain to fluids, acoustics, electromagnetic, and optics. Thanks to the recent advance in additive manufacturing, a complicated optimal design can be directly manufactured. However, the design optimization process involves an expensive physics model solution process. The most expensive part is a sequence of large-scale linear solves. Although a sparse linear system may arise, the size of the system hinders a rapid design process. There have been many attempts to reduce the cost of large-scale linear solves and they can be grouped to two categories: i) *allowing inexact linear solves* and ii) *reducing the number of iterations in Krylov subspace methods*.

To *allow inexact linear solves* in design optimization, Amir and his coauthors in [3] studied how to utilize the inexact solution of linear systems in the optimization process by considering specific convergence criteria and applying sensitivity correction terms to compliance and compliant mechanism problems. However, in order to extend their approach to other applications, such as stress-constrained problems, appropriate convergence criteria and sensitivity correction terms need to be developed. Gogu in [31] replaced high-fidelity linear solve with Reduced Order Models (ROMs) to accelerate the design optimization process. Basis was constructed on-the-fly by Gram-Schmidt process whenever the ROM residual was bigger than a tolerance set by a user. In order to set the tolerance relatively a large value, e.g., 0.1, the sensitivity correction terms were added to the ROM sensitivity as in [3]. However, the sensitivity correction terms required linear solves with full order model size. Those solves involved system matrices whose factorizations were already known if a direct solver was used. However, if linear systems are solved with iterative solvers, those factorizations are not available. Additionally, the ROM method was compared with an academic version of topology optimization algorithm written in MATLAB. Therefore, it is likely that the reported speed-up will be degraded when the ROM-based method is compared with the High-Performance Computing (HPC)-based Full Order Model (FOM) solves. Yoon in [65] used various model reduction techniques for frequency response problems. The

*Correspondence to: Lawrence Livermore National Laboratory, 7000 East Ave, Livermore, CA 94550, USA. E-mail: choi15@llnl.gov

†Lawrence Livermore National Laboratory is operated by Lawrence Livermore National Security, LLC, for the U.S. Department of Energy, National Nuclear Security Administration under Contract DE-AC52-07NA27344 and LLNL-JRNL-791183.

reduction methods were the mode superposition, Ritz vector, and quasi-static Ritz vector. All those ROMs mentioned above do not consider the reduced basis from the proper orthogonal decomposition, which is known to provide an optimal basis, given a data.

To *reduce the number of iterations in Krylov subspace methods*, a preconditioner is necessary. Although this paper does not focus on preconditioner (instead we use an existing preconditioner), the importance of a good preconditioner should not be ignored. An optimal and efficient preconditioner depends on each problem. Most widely used preconditioners include, but not limited to, Jacobi preconditioner, incomplete Cholesky factorization [32], Schur complement-based ones [21, 52], and multi-grid methods [6]. Another way of reducing the number of iterations in Krylov subspace methods is to use a recycling approach. The recycling approach has been mainly developed in numerical linear algebra and optimization communities, but some of the approaches were applied in topology optimization problems. For example, Wang and his coauthors in [64] used MINRES [50] with recycling to accelerate the solution process of both symmetric positive-definite and indefinite systems. Scaling of stiffness was used to bring down the condition number of stiffness matrix. They used incomplete Cholesky factorization as a preconditioner. However, the recycling subspace was taken from the solutions of previous linear solves, not from reduced basis of previous solution, resulting in a bigger recycling space. Unlike Wang’s work, Carlberg and his coauthors in [17] and Nguyen and Chen in [47] used reduced basis of previous solutions, which is a compact representation of previous solutions. Thus, they were able to keep the dimension of recycling subspace small and still reduce the number of iterations.

We present a novel ROM-based design optimization algorithm. It is motivated by the following characteristics of the optimization process: The gradient-based optimization solvers start with an initial design and explore the design space until it finds an optimal solution that satisfies the KKT conditions. In the beginning of the optimization process, the change of design variables is large, indicating that the linear solves at this stage do not have to be solved precisely. This is exactly the motivation for several gradient-based optimization algorithms that introduce various inexactness to accelerate the optimization process (e.g., see [7, 33, 15]). The inexactness allows us to replace FOM with a ROM in the beginning of the optimization process where ROM can provide an approximate solution much faster than the corresponding FOM. On the other hand, as the optimization process gets near the end, the change in design variables is small and a precise solution of each linear solve is required for a guarantee of the convergence to a local optimum. For this stage of the optimization process, we will use Krylov subspace methods with ROM-recycling space that is able to solve for an accurate enough solution with a reduced number of iterations. The combination of *the inexact ROMs* in the beginning and *the Krylov subspace methods with ROM-recycling* near the convergence can accelerate the overall topology optimization process and maximize the usage of ROMs.

Some additional features and contributions of our method are detailed in the following list:

- Incremental Singular Value Decomposition (SVD) and Gram-Schmidt orthogonalization are used to determine the reduced basis on-the-fly.
- Conjugate gradient with ROM-based recycling and Algebraic Multi-Grid (AMG) preconditioner are used to reduce the number of linear solve iterations.
- Our ROM-based design optimization algorithm quickly finds a local optimal design that satisfies a necessary optimality condition, i.e., the Karush-Kuhn-Tucker (KKT) conditions.
- The norm of the KKT conditions are used to determine if the ROM can replace the FOM or not.
- Our method is applied to a broad range of numerical examples of structural topology optimization: compliance minimization with single and multiple load cases and stress-constrained optimization with von Mises stress criterion.
- Both structured and unstructured meshes are tested in numerical experiments. Our method is able to accelerate the problems with both structured and unstructured meshes, but more so for the problems with unstructured mesh.
- Our proposed method is general enough so that it is applicable not only to topology optimizations, but also to general design optimization and any PDE-constrained optimization problems.
- Fully parallel version is implemented in C++ production code, developed at LLNL.

The rest of the paper is organized in the following way: Section 2 presents a topology optimization formulation as an example of Partial Differential Equation (PDE)-constrained design optimization and its solution methodology. Section 3 presents the interior-point method as an example of optimization solvers that uses the norm of the KKT conditions as stopping criteria. Section 4 explains how to construct an optimal reduced basis efficiently, using incremental factorization algorithms. Section 5 shows two ways of utilizing the reduced basis to accelerate the linear system solve process. In Section 5.1, the first one, i.e., a projection-based reduced order model ROM is introduced. In Section 5.2, the second one, i.e., a preconditioned conjugate gradient method with ROM-recycling is explained. Various numerical examples of structural topology optimization problems are shown to demonstrate the advantages of our method in Section 6. Section 7 concludes with summary and future directions.

1.1 Notations

Scalars are denoted by lowercase letters, e.g., a . Vectors are denoted by boldface lowercase letters, e.g., \mathbf{a} , and its i -th element by lowercase letter subscripted with an index, e.g., a_i . Matrices are denoted by boldface uppercase letters, e.g., \mathbf{A} , and its (i, j) -th element by lowercase letter subscripted with two indices, e.g., a_{ij} . The cardinality of a subspace, \mathcal{A} , is denoted as $|\mathcal{A}|$. The real number space is denoted as \mathbb{R} and positive real number space as \mathbb{R}_+ . The range space of \mathbf{A} is denoted as $\text{range}(\mathbf{A})$. The 2-norm of a vector is defined as $\|\mathbf{a}\|_2 := \sqrt{\sum_i a_i^2}$, 1-norm of a vector is defined as $\|\mathbf{a}\|_1 := \sum_i |a_i|$, and the infinity norm of a vector is defined as $\|\mathbf{a}\|_\infty := \max_i |a_i|$.

2 Topology optimization

As an example of PDE-constrained design optimization, we consider a structural topology optimization problem. However, our method is general enough to be applicable to a broad class of design optimization problems. A structural topology optimization finds the material distribution that minimizes an objective function, subject to m constraints. The material distribution is determined by the discretized volume fraction variables $\boldsymbol{\mu} \in \mathbb{R}^{N_d}$ that can take any value between 0 (void) and 1 (solid material) for each non-overlapping element Ω_i , $i \in \mathbb{N}(N_d)$, where $\mathbb{N}(N_d) := \{1, \dots, N_d\}$, in design domain Ω , and the number of elements N_d (i.e., $\bar{\Omega} = \cup_{i=1}^{N_d} \bar{\Omega}_i$ and $\Omega_i \cap \Omega_j = \emptyset$ for $i \neq j$). This optimization problem can be mathematically formulated as:

$$\begin{aligned}
 & \underset{\boldsymbol{\mu} \in \mathbb{R}^{N_d}}{\text{minimize}} && f(\mathbf{w}(\boldsymbol{\mu}), \boldsymbol{\mu}) \\
 & \text{subject to} && g_0(\boldsymbol{\mu}) = \sum_i \mu_i v_i - v_u \leq 0 \\
 & && g_i(\mathbf{w}(\boldsymbol{\mu}), \boldsymbol{\mu}) \leq 0, \quad i \in \mathbb{N}(m) \\
 & && \mathbf{r}(\mathbf{w}; \boldsymbol{\mu}) = \mathbf{0} \\
 & && \mathbf{0} \leq \boldsymbol{\mu} \leq \mathbf{1}
 \end{aligned} \tag{1}$$

where $f : \mathbb{R}^{N_s} \times \mathbb{R}^{N_d} \rightarrow \mathbb{R}$ denotes an objective function, v_i denotes the volume of element Ω_i , v_u denotes the upper bound for the total volume of the material. Optimization (1) includes a volume constraint $g_0 \leq 0$ and possibly m other nonlinear constraints $g_i \leq 0$, $i \in \mathbb{N}(N_d)$. Finally, $\mathbf{w} : \mathbb{R}^{N_d} \rightarrow \mathbb{R}^{N_s}$ denotes a discretized displacement state vector function that depends implicitly on the volume fraction variables through the state equation residual function, $\mathbf{r} : \mathbb{R}^{N_s} \times \mathbb{R}^{N_d} \rightarrow \mathbb{R}^{N_s}$. For example, the discretized PDE residual function for linear elasticity is defined as

$$\mathbf{0} = \mathbf{r}(\mathbf{w}; \boldsymbol{\mu}) := \mathbf{K}(\boldsymbol{\mu})\mathbf{w} - \mathbf{b}(\boldsymbol{\mu}), \tag{2}$$

where $\mathbf{K} : \mathbb{R}^{N_d} \rightarrow \mathbb{R}^{N_s \times N_s}$ denotes a parameter dependent stiffness matrix (note $\mathbf{K} = \frac{\partial \mathbf{r}}{\partial \mathbf{w}}$) and $\mathbf{b} : \mathbb{R}^{N_d} \rightarrow \mathbb{R}^{N_s}$ is a parameter-dependent right-hand-side vector for linear elasticity equation via finite element discretization (see Section 2 of [37]). Note that the system of equations (2) need to be solved to evaluate f and g_i . The solution process of (2) is labeled as the *physics PDE solve* in the topology optimization flow chart (see Figure 1a).

Various quantities of interest can be considered as the objective, f , and constraint, g_i , functions in the structural topology optimization. For example, they include the compliance, i.e., $\mathbf{w}^T \mathbf{b} = \mathbf{w}^T \mathbf{K} \mathbf{w}$ in discretized form [8], moment of inertia [39], and various yield stress criteria, e.g., von Mises stress [43] and Drucker-Prager for concrete materials [45].

In early days of topology optimization development, the checkerboard problem, i.e., patches of alternating void and material elements, was a major problem [25, 38, 60]. This problem is related to ensuring the well-posed and mesh-independent solutions. It can be addressed by introducing the various density filters: the cone filters [12, 14] and the PDE filters [42, 40]. These filters act as smoothing and mixing tools of the irregular density variables, making individual density values dependent on neighboring elements. Therefore, it should be noted that perimeter and slope constraints can also be used to avoid the checkerboard patterns. Another possible filter is to apply the corresponding mass matrix to the density variables, which we call the mass filter. The minimum length scale of the mass matrix filter is imposed by the element size. In this paper, we use either the mass matrix filter or the following Helmholtz type diffusion operator in [42]:

$$-r^2 \Delta \rho + \rho = \mu, \tag{3}$$

where the filter radius, $r > 0$ controls the minimum length scale and ρ denotes a filtered volume fraction variable. Note that ρ depends on μ implicitly through (3). Unfortunately, these filtering methods introduce grey areas between solid and void regions. These grey areas can be minimized by reducing the filter radius.

The Solid Isotropic Material with Penalization (SIMP) or power-law approach is developed to ensure void-solid solutions by penalizing intermediate volume fraction variables [66, 46, 9]. In the SIMP method, the volume fraction

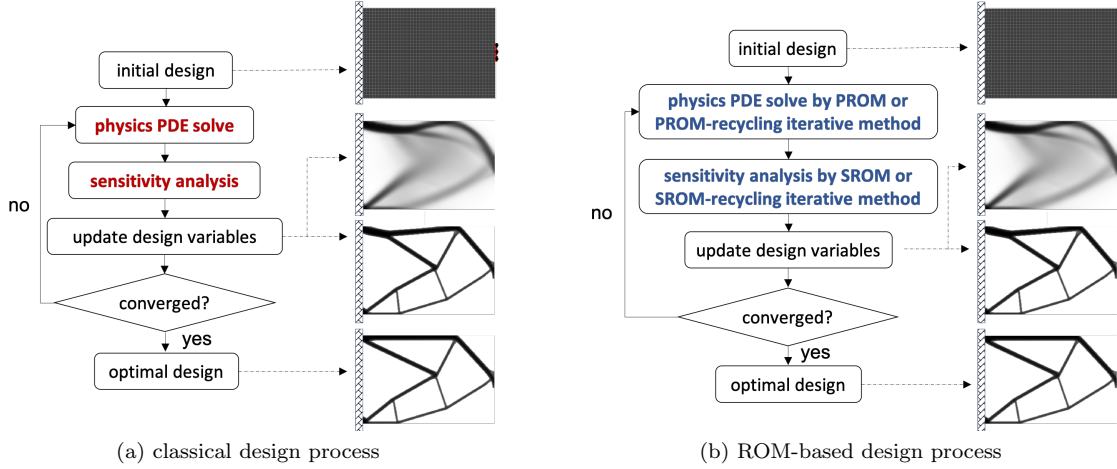


Figure 1: Comparison of classical and ROM-based design optimization flow charts in gradient-based optimization solvers. Basically, the ROM-based design process replaces the computationally expensive *PDE solves* and *sensitivity analysis* with either corresponding ROMs or ROM-recycling iterative methods. In (b), PROM refers to a ROM for *physics PDE solve* and SROM refers to a ROM for *sensitivity analysis*.

variable and the material property is related by

$$E(\rho_i) = \rho_i^s E_0, \quad (4)$$

where $s \in (1, \infty)$ denotes the penalization parameter, $E_0 \in \mathbb{R}$ denotes the Young's modulus of solid material, and finally, $E \in \mathbb{R}$ denotes the penalized Young's modulus. A similar approach can be applied for stress-constrained topology optimization problems to address the *singularity* problem [43], i.e.,

$$T(\rho_i) = \rho_i^q T_0, \quad (5)$$

where $q \in (0, 1)$ denotes the penalization parameter, $T_0 \in \mathbb{R}$ denotes a stress quantity of solid material, and finally, $T \in \mathbb{R}$ denotes the relaxed stress. An alternative to the SIMP method is also available, e.g., the RAMP (Rational Approximation of Material Properties) method [61] and the explicit penalization method [1, 2]. As a result, these penalized material properties are used to set up, for example, the state equations (2) and various quantity of interests for f and g_i .

A gradient-based optimization solver requires gradient $\frac{df}{d\mu} \in \mathbb{R}^{N_d}$ and Jacobians $\frac{dg_i}{d\mu} \in \mathbb{R}^{N_d}$, $i \in \mathbb{N}(m)$. The *sensitivity analysis* in Figure 1a, is the step when those derivatives are computed. They can be computed via chain rule. For example, the chain rule for the objective function gives:

$$\frac{df}{d\mu} = \frac{\partial f}{\partial \mu} + \frac{\partial f}{\partial \mathbf{w}} \frac{d\mathbf{w}}{d\mu}, \quad (6)$$

where $\frac{d\mathbf{w}}{d\mu} \in \mathbb{R}^{N_s \times N_d}$ can be obtained from the derivative of the linear PDE residual:

$$\mathbf{0} = \frac{d\mathbf{r}}{d\mu} = \frac{\partial \mathbf{r}}{\partial \mu} + \frac{\partial \mathbf{r}}{\partial \mathbf{w}} \frac{d\mathbf{w}}{d\mu}, \quad (7)$$

$$= \left(\frac{d\mathbf{K}}{d\mu} \mathbf{w} - \frac{d\mathbf{b}}{d\mu} \right) + \mathbf{K}(\mu) \frac{d\mathbf{w}}{d\mu}. \quad (8)$$

The direct method solves Eq. (7) “directly” for $\frac{d\mathbf{w}}{d\mu}$. Note that the direct method requires N_d linear system solves for N_d different right hand sides regardless of the number of quantity of interests, i.e., $m + 1$. Then, it substitutes $\frac{d\mathbf{w}}{d\mu}$ to (6) and obtains the gradient, $\frac{df}{d\mu}$. On the other hand, *the adjoint method* solves for Lagrange multipliers, $\boldsymbol{\lambda}$, by solving the following linear adjoint system,

$$\left(\frac{\partial \mathbf{r}}{\partial \mathbf{w}} \right)^T \boldsymbol{\lambda} = \frac{\partial f}{\partial \mathbf{w}}, \quad (9)$$

then computes the gradient

$$\frac{df}{d\boldsymbol{\mu}} = \frac{\partial f}{\partial \boldsymbol{\mu}} - \boldsymbol{\lambda} \frac{\partial \mathbf{r}}{\partial \boldsymbol{\mu}}. \quad (10)$$

Note that the adjoint method requires one linear adjoint system solve for each quantity of interest (i.e., $m + 1$ linear adjoint system solves) regardless of the number of decision variables. Therefore, one needs to use the adjoint method if $m + 1 < N_d$, while the direct method is preferred otherwise. In density-based structural topology optimization, N_d is proportional to the number of elements of spatial discretization, so it is likely to be larger than $m + 1$. Therefore, the adjoint method is preferred to the direct method in topology optimization. For more detailed review on topology optimization, please see these survey papers [24, 59, 60].

The gradient-based optimization algorithms need to solve a sequence of linear systems:

$$\mathbf{A}_k \mathbf{u}_k = \mathbf{b}_k, \quad (11)$$

where the unknown variables are $\mathbf{u}_k = \mathbf{w}_k$ for the PDE solve in (2), $\mathbf{u}_k = \frac{\partial \mathbf{r}_k}{\partial \mathbf{w}_k}$ for the direct sensitivity solve in (7), and $\mathbf{u}_k = \boldsymbol{\lambda}_k$ for the adjoint system in (9). The subscript k in \mathbf{w}_k , \mathbf{r}_k , and $\boldsymbol{\lambda}_k$ indicates k th PDE, direct, and adjoint linear solves, respectively. These linear solves are necessary when objective, constraints, and their sensitivities need to be evaluated. Although a sparse linear system arises, the size and number of the linear system solution process hinders a rapid design process. These solves are the most expensive part of the optimization process. For example, the computational time for the total optimization process for the wind turbine blade design problem in Section 6.1.2 is 2.1 hours, while the time for the linear solves is 1.7 hours, taking about 81% of the total cost. Therefore, developing a method of accelerating the sequence of large-scale linear solve is essential. We achieve this by the ROM-based design optimization process described in Figure 1b. The ROM-based design optimization process enables to reduce 1.7 hours of linear system solving time to 0.48 hours for the same blade design problem, bringing down the cost of linear solves in the optimization process significantly. Our method replaces the computationally expensive linear system solves occurred in *physics PDE solve* and *sensitivity analysis* indicated in Figure 1a with either *the inexact ROM solve* or *the ROM-recycling iterative solve*, e.g., see Figure 1b. The choice between the inexact ROM or ROM-recycling iterative solve is determined by the norm of the KKT conditions.¹ In the following section, the KKT conditions in the context of the interior point method are derived.

3 Interior point method

There are several gradient-based optimization algorithms that can solve Problem (1). For structural design optimizations, the Method of Moving Asymptotes (MMA) [62], the Optimality Criterion (OC) [55, 56, 66, 4], and CONLIN [28] are popular gradient-based algorithms. However, these algorithms are not robust in terms of the KKT conditions [54]. Unfortunately, this implies that these algorithms are not suitable to obtain a local minimum. Our interest is in the optimization algorithms that can achieve the KKT conditions. Such algorithms include, but not limited to, the Sequential Quadratic Programming (SQP) [11], the Interior Point Methods (IPMs) [29, 30, 63], the trust region methods based on IPMs [16], and the augmented Lagrangian methods [22]. We focus on the IPMs and its KKT conditions because we use IPOPT [63] in our numerical experiment section. However, it is worthwhile to note that our method can be applied to any gradient-based optimization algorithms that find a KKT point.

Introducing the following dummy variables and equations:

$$q_0 = -g_0, \quad q_0 \geq 0 \quad (12)$$

$$q_i = -g_i, \quad q_i \geq 0, \quad i \in \mathbb{N}(m) \quad (13)$$

$$\nu_j = 1 - \mu_j, \quad \nu_j \geq 0, \quad j \in \mathbb{N}(N_d), \quad (14)$$

and setting $\mathbf{x}^T = (\boldsymbol{\mu}^T \quad \mathbf{q}^T \quad \boldsymbol{\nu}^T)$, Problem (1) can be transformed to the following general formulation:

$$\begin{aligned} & \underset{\mathbf{x} \in \mathbb{R}^{N_x}}{\text{minimize}} && f(\mathbf{x}) \\ & \text{subject to} && \mathbf{h}(\mathbf{x}) = \mathbf{0} \\ & && \mathbf{x} \geq \mathbf{0}, \end{aligned} \quad (15)$$

¹The KKT conditions are the first-order optimality conditions if constraint qualifications are satisfied. Many optimization algorithms use these conditions to look for a local minimum. A sufficient condition for the local minimum is to have non-negative eigenvalues at the point.

where $N_x = 2N_d + m + 1$ and $\mathbf{h}(\mathbf{x}) = \mathbf{g}(\mathbf{x}) + \mathbf{q}$. To solve (15), IPM solves a sequence of barrier problems with the homotopy parameter $\omega \in \mathbb{R}_+$ decreasing to zero:

$$\begin{aligned} \underset{\mathbf{x} \in \mathbb{R}^{N_x}}{\text{minimize}} \quad & f(\mathbf{x}) - \omega \sum_{i=1}^{N_x} \ln(x_{(i)}) \\ \text{subject to} \quad & \mathbf{h}(\mathbf{x}) = \mathbf{0}. \end{aligned} \quad (16)$$

Defining dummy variables, $z_i = \omega/x_i$, $i \in \mathbb{N}(N_x)$, the KKT conditions for (16) are

$$\nabla f(\mathbf{x}) + \nabla \mathbf{h}(\mathbf{x})\boldsymbol{\eta} - \mathbf{z} = \mathbf{0} \quad (17)$$

$$\mathbf{h}(\mathbf{x}) = \mathbf{0} \quad (18)$$

$$\mathbf{X}\mathbf{Z}\mathbf{e} - \omega\mathbf{e} = \mathbf{0}, \quad (19)$$

where $\boldsymbol{\eta} \in \mathbb{R}^{m+1}$ denotes a Lagrange multiplier vector, $\mathbf{e} \in \mathbb{R}^{N_x}$ denotes a vector with all the element values being one, and $\mathbf{X}, \mathbf{Z} \in \mathbb{R}^{N_x \times N_x}$ are diagonal matrices whose diagonals are \mathbf{x} and \mathbf{z} , respectively. The interior point method follows the homotopy procedure where the barrier problem (16) is solved for the unknowns, $(\mathbf{x}, \mathbf{z}, \boldsymbol{\eta})$, with a fixed $\omega > 0$, then decreases the value of ω , and solves the barrier problem with the previous solution as an initial guess. We repeat this process as the value of ω decreases to a small positive value close to zero. This process is justified by the fact that Eqs. (17), (18), and (19) are the KKT conditions for Problem (15) if $\omega = 0$ and $\mathbf{x}, \mathbf{z} \geq \mathbf{0}$.² Therefore, when the homotopy procedure is complete, the solution to the barrier problem is a good approximate solution to Problem (15).

One can include all the KKT equality conditions to define their norms: the stationarity, primal feasibility, and complementarity conditions. The IPOPT defines the norm of the KKT conditions in the following way:

$$r_{\text{kkt}} = \max \left(\frac{\|\nabla f(\mathbf{x}) + \nabla \mathbf{h}(\mathbf{x})\boldsymbol{\eta} - \mathbf{z}\|_{\infty}}{s_d}, \|\mathbf{h}(\mathbf{x})\|_{\infty}, \frac{\|\mathbf{X}\mathbf{Z}\mathbf{e}\|_{\infty}}{s_c} \right), \quad (20)$$

where $s_d, s_c \geq 1$ are defined as

$$s_d = \max \left(s_{\max}, \frac{\|\boldsymbol{\eta}\|_1 + \|\mathbf{z}\|_1}{m + N_x} \right) / s_{\max}, \quad s_c = \max \left(s_{\max}, \frac{\|\mathbf{z}\|_1}{N_x} \right) / s_{\max}. \quad (21)$$

This makes sure that a component of the optimality error is scaled, when the average value of the multipliers is larger than a fixed number $s_{\max} \geq 1$. We use $s_{\max} = 100$ as in IPOPT. The IPM software uses this norm or its variants to determine the convergence of the optimization process. The value of the KKT norm indicates how close the current point is to an optimal point.³ In ROM-based design optimization algorithm, FOM is completely replaced with ROM when the current point is far from an optimal point because the system does not need to be solved precisely. Therefore, we will use r_{kkt} as a measure to determine if the ROM replaces the corresponding FOM or not.

4 Reduced basis

The topology optimization solves a sequence of linear system of equations (11) that generates a sequence of solutions, \mathbf{u}_k .⁴ The sequence of solutions converges to an optimal solution, \mathbf{u}_* if the problem is feasible. Additionally, as the optimization process is close to the end, the sequence of solutions does not change much, i.e., $\|\mathbf{u}_k - \mathbf{u}_{k+1}\|_2 \leq \epsilon$ for $k > K > 0$ with a sufficiently large number K and a small number ϵ . Therefore, finding the solution \mathbf{u}_k within the subspace spanned by the previous ℓ solutions, $\mathcal{A}_{k-1}^{\ell} := \text{range}(\mathbf{A}_{k-1}^{\ell})$, $\mathbf{A}_{k-1}^{\ell} := [\mathbf{u}_{k-\ell}, \dots, \mathbf{u}_{k-1}] \in \mathbb{R}^{N_s \times \ell}$, must give a good approximation to \mathbf{u}_k . There are several ways of obtaining a basis Φ_k for \mathcal{A}_{k-1}^{ℓ} , but not limited to,

- a simple collection of previous ℓ solutions, i.e., $\Phi_k = \mathbf{A}_{k-1}^{\ell}$
- an orthogonalized basis, e.g., via QR decomposition
- a Proper Orthogonal Decomposition (POD) basis.

The first choice is the simplest, but as the optimization process converges to an optimal solution, it generates a sequence of solution vectors that are almost linearly dependent. That causes the ill-condition of the reduced system. Therefore, orthogonalization process, such as QR decomposition, is necessary, which is the second choice above. The

²The KKT conditions of (15) include the stationarity condition (17), the primal feasibility conditions (18) and $\mathbf{x} \geq \mathbf{0}$, the complementarity condition (19) with $\omega = 0$, and duality condition, $\mathbf{z} \geq \mathbf{0}$.

³A large r_{kkt} indicates that the point is far from an optimal point. A small r_{kkt} indicates the point is close to an optimal.

⁴Most gradient-based optimization algorithms find a local minimum.

Algorithm 1 Incremental QR, $\Phi_{-1} = []$

$\Phi_k = \text{incrementalQR}(\mathbf{c}, \epsilon_{\text{QR}}, k, \Phi_{k-1}, r_{\text{max}})$

Input: $\mathbf{c}, \epsilon_{\text{QR}}, k, \Phi_{k-1}, r_{\text{max}}$

Output: Φ_k

- 1: **if** $k = 0$ **then**
 - 2: $\Phi_0 \leftarrow \mathbf{c} / \|\mathbf{c}\|$
 - 3: **else if** $0 < r_{k-1} \leq r_{\text{max}}$ **then**
 - 4: $\Phi_k \leftarrow \text{incrementalQRupdate}(\mathbf{c}, \epsilon_{\text{QR}}, \Phi_{k-1})$, i.e., apply Algorithm 2
 - 5: **else**
 - 6: $\Phi_{k-1} \leftarrow \Phi_{k-1}(:, 2 : r_{\text{max}})$
 - 7: $\Phi_k \leftarrow \text{incrementalQRupdate}(\mathbf{c}, \epsilon_{\text{QR}}, \Phi_{k-1})$, i.e., apply Algorithm 2
 - 8: **end if**
-

Algorithm 2 Incremental QR update

$\Phi_k = \text{incrementalQRupdate}(\mathbf{c}, \epsilon_{\text{QR}}, \Phi_{k-1})$

Input: $\mathbf{c}, \epsilon_{\text{QR}}, \Phi_{k-1}$

Output: Φ_k

- 1: $\mathbf{j} \leftarrow \mathbf{c} - \Phi_k \Phi_k^T \mathbf{c}$
 - 2: **if** $\|\mathbf{j}\| > \epsilon_{\text{QR}}$ **then**
 - 3: $\Phi_k \leftarrow [\Phi_{k-1} \quad \mathbf{j} / \|\mathbf{j}\|]$
 - 4: **else**
 - 5: $\Phi_k \leftarrow \Phi_{k-1}$
 - 6: **end if**
-

third choice above is motivated by POD. The basis from POD is an optimally compressed representation of \mathcal{A}_{k-1} in a sense that it minimizes the difference between the original snapshot matrix and the projected one onto the subspace spanned by the basis, Φ_k :

$$\underset{\Phi_k \in \mathbb{R}^{N_s \times r_k}, \Phi_k^T \Phi_k = \mathbf{I}_{r_k}}{\text{minimize}} \quad \left\| \mathbf{A}_{k-1}^\ell - \Phi_k \Phi_k^T \mathbf{A}_{k-1}^\ell \right\|_F^2, \quad (22)$$

where $\|\cdot\|_F$ denotes the Frobenius norm and r_k denotes the rank of the basis. The solution of POD can be obtained by setting $\Phi_k = \mathbf{U}(:, 1 : r_k)$ in MATLAB notation, where \mathbf{U} is the left singular matrix of the following thin Singular Value Decomposition (SVD):

$$\mathbf{A}_{k-1}^\ell = \mathbf{U} \mathbf{\Sigma} \mathbf{V}^T, \quad (23)$$

where $\mathbf{U} \in \mathbb{R}^{N_s \times \ell}$ and $\mathbf{V} \in \mathbb{R}^{\ell \times \ell}$ are orthogonal matrices and $\mathbf{\Sigma} \in \mathbb{R}^{\ell \times \ell}$ is a diagonal matrix with singular values on its diagonals. SVD can order its modes from a most dominant mode to a least dominant mode. Thus, the first SVD basis vector is more important than the last SVD basis vector, making it easy to truncate and use only dominant modes in reduced basis. POD is related to principal component analysis in statistics [36] and Karhunen–Loève expansion [44] in stochastic analysis. Since the objective function in (22) does not change even though Φ_k is post-multiplied by an arbitrary $r_k \times r_k$ orthogonal matrix, the POD procedure seeks the optimal r_k -dimensional subspace that captures the snapshots in the least-squares sense. For more details on POD, we refer to [10, 35, 41].

We will choose either the second or third choice above to generate our basis. However, it is computationally expensive to perform either QR or SVD of the snapshot matrix from scratch every time it is updated. For example, the computational cost of SVD for $\mathbf{A}_{k-1}^\ell \in \mathbb{R}^{N_s \times \ell}$ is $O(N_s^2 \ell)$. Considering a large N_s , this cost is too much. Therefore, we use incremental algorithms where an efficient update to the previous decomposition is done when a new snapshot vector is added. For the QR decomposition, the Gram-Schmidt orthogonalization perfectly fits into the incremental framework, i.e., see Algorithm 1. The inputs for the incremental QR in Algorithm 1 include snapshot vector \mathbf{c} , threshold for linear dependency ϵ_{QR} , index k , previous basis matrix Φ_{k-1} , and maximum allowable rank of the basis matrix r_{max} . The incremental QR starts with $k = 0$ with an empty basis matrix $\Phi_{-1} = []$. For $k = 0$, it simply normalizes the snapshot vector and set Φ_0 . For $k > 0$, it applies the incremental QR update in Algorithm 2 as long as the rank of the basis matrix does not exceed the maximum allowable rank r_{max} . If it exceeds the maximum allowable rank, then Algorithm 1 throws away the first basis vector in Φ_{k-1} . Then it applies the incremental QR update in Algorithm 2. In the incremental QR update in Algorithm 2, if snapshot vector \mathbf{c} can be spanned by the basis vectors in Φ_{k-1} , then we set $\Phi_k = \Phi_{k-1}$. Otherwise, we include the effect of \mathbf{c} to Φ_k .

For SVD, we use the incremental SVD in Algorithms 3 and 4. They were initially developed in [49]. The algorithm

Algorithm 3 Initializing incremental SVD

 $[\Phi_k, \mathbf{s}, \Psi] = \text{initializingIncrementalSVD}(\mathbf{c}, \epsilon_{\text{SVD}}, k)$
Input: $\mathbf{c}, \epsilon_{\text{SVD}}, k$
Output: Φ_k, \mathbf{s}, Ψ

- 1: **if** $\|\mathbf{c}\| > \epsilon_{\text{SVD}}$ **then**
 - 2: $\mathbf{s} \leftarrow \lceil \|\mathbf{c}\| \rceil$, $\Phi_k \leftarrow \mathbf{c}/s_1$, and $\Psi \leftarrow [1]$
 - 3: **else**
 - 4: $\mathbf{s} \leftarrow []$, $\Phi_k \leftarrow []$, and $\Psi \leftarrow []$
 - 5: **end if**
-

is initialized with the *initializing incremental SVD* in Algorithm 3. Then the following factorization is available for a rank-one update of the existing SVD [13]:

$$[\Phi_{k-1} \Sigma_{k-1} \Psi_{k-1}^T \quad \mathbf{c}] = [\Phi_{k-1} \quad (\mathbf{I} - \Phi_{k-1} \Phi_{k-1}^T) \mathbf{c}/p] \begin{bmatrix} \Sigma_{k-1} & \Phi_{k-1}^T \mathbf{c} \\ \mathbf{0} & p \end{bmatrix} \begin{bmatrix} \Psi_{k-1} & \mathbf{0} \\ \mathbf{0} & 1 \end{bmatrix}^T \quad (24)$$

$$= [\Phi_{k-1} \quad \mathbf{j}] \begin{bmatrix} \Sigma_{k-1} & \ell \\ \mathbf{0} & p \end{bmatrix} \begin{bmatrix} \Psi_{k-1} & \mathbf{0} \\ \mathbf{0} & 1 \end{bmatrix}^T, \quad (25)$$

where $\ell = \Phi_{k-1}^T \mathbf{c}$ denotes a reduced coordinate of \mathbf{c} , $p = \|\mathbf{c} - \Phi_{k-1} \ell\|$ denotes the norm of the difference between \mathbf{c} and the projected one, and $\mathbf{j} = (\mathbf{c} - \Phi_{k-1} \ell) / p$ denotes a new orthogonal vector due to the incoming vector, \mathbf{c} . Let

$$\mathbf{Q} = \begin{bmatrix} \Sigma_{k-1} & \ell \\ \mathbf{0} & p \end{bmatrix}. \quad (26)$$

The matrix, $\mathbf{Q} \in \mathbb{R}^{(r_{k-1}+1) \times (r_{k-1}+1)}$, is almost diagonal except for ℓ in the upper right block and also its size is not in $O(N_s)$. Thus, the SVD of \mathbf{Q} is computationally fast. The cost is $O((r_{k-1}+1)^3)$, which is a lot cheaper than $O(N_s^2 \ell)$. Let the SVD of \mathbf{Q} be

$$\mathbf{Q} = \bar{\Phi}_{k-1} \bar{\Sigma}_{k-1} \bar{\Psi}_{k-1}, \quad (27)$$

where $\bar{\Phi}_{k-1} \in \mathbb{R}^{(r_{k-1}+1) \times (r_{k-1}+1)}$ denotes the left singular matrix, $\bar{\Sigma}_{k-1} \in \mathbb{R}^{(r_{k-1}+1) \times (r_{k-1}+1)}$ denotes the singular value matrix, and $\bar{\Psi}_{k-1} \in \mathbb{R}^{(r_{k-1}+1) \times (r_{k-1}+1)}$ denotes the right singular matrix of \mathbf{Q} . Replacing \mathbf{Q} in Eq. (25) with (27) gives

$$[\Phi_{k-1} \Sigma_{k-1} \Psi_{k-1}^T \quad \mathbf{c}] = [\Phi_{k-1} \quad \mathbf{j}] \bar{\Phi}_{k-1} \bar{\Sigma}_{k-1} \bar{\Psi}_{k-1} \begin{bmatrix} \Psi_{k-1} & \mathbf{0} \\ \mathbf{0} & 1 \end{bmatrix}^T \quad (28)$$

$$= \Phi_k \Sigma_k \Psi_k^T, \quad (29)$$

where $\Phi_k = [\Phi_{k-1} \quad \mathbf{j}] \bar{\Phi}_{k-1} \mathbb{R}^{N_s \times (r_k)}$ denotes the updated left singular matrix, $\Sigma_k = \bar{\Sigma}_{k-1} \in \mathbb{R}^{r_k \times r_k}$ denotes the updated singular value matrix, and $\Psi_k = \begin{bmatrix} \Psi_{k-1} & \mathbf{0} \\ \mathbf{0} & 1 \end{bmatrix} \bar{\Psi}_{k-1} \in \mathbb{R}^{r_k \times r_k}$ denotes the updated right singular matrix.

Algorithm 4 checks if \mathbf{c} is numerically linearly dependent on the current basis vectors. If $p < \epsilon_{\text{SVD}}$, then we consider it is linearly dependent. Thus, we set $p = 0$ in \mathbf{Q} , i.e., Line 9 of Algorithm 4. Then we only update the first r_{k-1} components of the singular matrices in Line 14 of Algorithm 4. Although the orthogonality of the updated basis matrix, Φ_k , must be guaranteed theoretically by the product of two orthogonal matrices in Line 14 or 16 of Algorithm 4, it is not guaranteed numerically. Thus, we heuristically check the orthogonality in Lines 18-21 of Algorithm 4 by checking the inner product of the first and last columns of Φ_k . If the orthogonality fails, then we orthogonalize them by the QR factorization. Also, we limit the dimension of the basis to be less than or equal to r_{max} because it is not necessary to include data far away from the current point of the optimization process in the reduced basis. See Line 1 of Algorithm 4.

Once the basis matrix Φ_k is constructed, it can be used to construct ROM or recycling subspace of Krylov iterative methods. Specifically, Section 5 illustrates the flow chart of the ROM-based linear system acceleration scheme and Section 5.1 explains how Φ_k is used to construct a projection-based ROM. Section 5.2 shows the preconditioned conjugate gradient method with ROM-recycling.

Algorithm 4 Incremental SVD, $\Phi_{-1} = []$

 $[\Phi_k, \mathbf{s}, \Psi] = \text{incrementalSVD}(\mathbf{c}, \epsilon_{\text{SVD}}, \Phi_{k-1}, \mathbf{s}, \Psi, k)$ **Input:** $\mathbf{c}, \epsilon_{\text{SVD}}, \Phi_{k-1}, \mathbf{s}, \Psi, k$ **Output:** Φ_k, \mathbf{s}, Ψ

```
1: if  $r_{k-1} = 0$  or  $r_{k-1} = r_{\max}$  then
2:    $[\Phi_k, \mathbf{s}, \Psi] = \text{initializingIncrementalSVD}(\mathbf{c}, \epsilon_{\text{SVD}}, k)$ , i.e., apply Algorithm 3
3: end if
4:  $\ell \leftarrow \Phi_{k-1}^T \mathbf{c}$ 
5:  $p \leftarrow \sqrt{\mathbf{c}^T \mathbf{c} - \ell^T \ell}$ 
6:  $\mathbf{j} \leftarrow (\mathbf{c} - \Phi_{k-1} \ell) / p$ 
7:  $\mathbf{Q} \leftarrow \begin{bmatrix} \text{diag}(\mathbf{s}) & \ell \\ \mathbf{0} & p \end{bmatrix}$ 
8: if  $p < \epsilon_{\text{SVD}}$  then
9:    $\mathbf{Q}_{\text{end,end}} \leftarrow \mathbf{0}$ 
10: end if
11:  $[\bar{\Phi}_{k-1}, \bar{\Sigma}_{k-1}, \bar{\Psi}_{k-1}] \leftarrow \text{SVD}(\mathbf{Q})$ 
12:
13: if  $p < \epsilon_{\text{SVD}}$  then
14:    $\Phi_k \leftarrow \Phi_{k-1} \bar{\Phi}_{k-1:1:r_{k-1}, 1:r_{k-1}}$ ,  $\mathbf{s}_k \leftarrow \text{diag}(\bar{\Sigma}_{1:r_{k-1}, 1:r_{k-1}})$ , and  $\Psi_k \leftarrow \bar{\Psi}_{k-1:1:r_{k-1}, :}$ 
15: else
16:    $\Phi_k \leftarrow [\Phi_{k-1} \quad \mathbf{j}] \bar{\Phi}_{k-1}$ ,  $\mathbf{s}_k \leftarrow \text{diag}(\bar{\Sigma}_{k-1})$ , and  $\Psi_k \leftarrow \begin{bmatrix} \Psi_k & \mathbf{0} \\ \mathbf{0} & 1 \end{bmatrix} \bar{\Psi}_{k-1}$ 
17: end if
18: if  $\Phi_{k:,1}^T \Phi_{k:,\text{end}} > \min\{\epsilon_{\text{SVD}}, \epsilon \cdot m_\Phi\}$  then
19:    $[\bar{\mathbf{Q}}, \bar{\mathbf{R}}] \leftarrow QR\{\Phi_k\}$ 
20:    $\Phi_k \leftarrow \bar{\mathbf{Q}}$ 
21: end if
```

5 ROM-based linear system acceleration scheme

To alleviate the cost of solving the system of linear equations (11),⁵ we apply the *ROM-based linear system acceleration scheme*, described in Figure 2. The acceleration scheme starts with a ROM solve, which will be described in Section 5.1. If the ROM solution is good enough, then we use the ROM solution to update the design variables in Figure 1b. Otherwise, it invokes the ROM-recycling iterative method, which gives a precise solution in a fast manner. The precise solution, in turn, is used as a new snapshot vector to update the current ROM within the incremental algorithms of Section 4 as well as the design variables in the optimization process of Figure 1b. Section 5.1 shows how to build and solve ROMs. It also defines a residual norm of the ROM, r_{rom} , and a KKT conditions-related threshold, ϵ_{rom} . Section 5.2 describes PCG with ROM-recycling method as an example of ROM-recycling iterative method.

5.1 Projection-based ROM

Now we start to explain how the *ROM solve* is done in Figure 2. The projection-based model reduction reduces the dimension of the system in (11) by reducing the number of the unknowns. For that purpose, the reduced basis $\Phi_k \in \mathbb{R}^{N_s \times r_k}$ is used to approximate the solution variables as

$$\mathbf{u}_k \approx \tilde{\mathbf{u}}_k := \mathbf{u}_k^{\text{ref}} + \Phi_k \hat{\mathbf{u}}_k, \quad (30)$$

where $\hat{\mathbf{u}}_k \in \mathbb{R}^{r_k}$ denotes the reduced coordinates and $\mathbf{u}_k^{\text{ref}}$ denotes a reference solution vector. Choices for $\mathbf{u}_k^{\text{ref}}$ include zero vector and initial condition for time dependent problems. Substituting (30) into (11) and applying Galerkin projection lead to the following reduced system of equation:

$$\hat{\mathbf{A}}_k \hat{\mathbf{u}}_k = \hat{\mathbf{r}}_k, \Phi_k^T \mathbf{r}_k, \quad (31)$$

where $\hat{\mathbf{A}}_k := \Phi_k^T \mathbf{A}_k \Phi_k \in \mathbb{R}^{r_k \times r_k}$ denotes a reduced linear system operator and $\hat{\mathbf{r}}_k := \Phi_k^T (\mathbf{b}_j - \mathbf{A}_j \mathbf{u}_K^{\text{ref}}) \in \mathbb{R}^{r_k}$ denotes a reduced right-hand side vector. The costs of constructing $\hat{\mathbf{A}}_k$ and $\hat{\mathbf{r}}_k$ are at most $O(2(b_k + 1)r_k N_s + r_k^3)$ and

⁵More precisely speaking, to alleviate the cost of solving the system of linear equations in (2) and either (7) or (9)

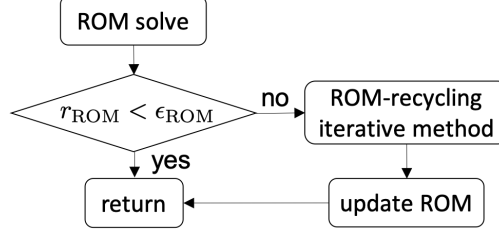


Figure 2: Flow chart of the ROM-based linear system acceleration scheme

$O(N_s r_k)$, respectively, assuming a banded structure in \mathbf{A}_k with its bandwidth, b_k . The construction of $\hat{\mathbf{A}}_k$ can be large depending on how large r_k and b_k are. There is a hyper-reduction technique available to reduce the construction cost of reduced operators although we do not apply it to our numerical examples. For example, see [18, 26, 20] for various hyper-reduction techniques.

The cost for the solution process of (31) is $O(r_k^3)$ for general methods. The solution to Eq. (31) can be re-substituted to (30) to recover the full size solution, $\tilde{\mathbf{u}}_k$. Since it is an approximation, the residual function value of $\tilde{\mathbf{u}}_k$ is most likely to be non-zero, i.e., $\mathbf{b}_k - \mathbf{A}_k \tilde{\mathbf{u}}_k \neq \mathbf{0}$. We define the following relative residual norm of the ROM to measure the accuracy of $\tilde{\mathbf{u}}_k$:

$$r_{\text{rom}} := \frac{\|\mathbf{b}_k - \mathbf{A}_k \tilde{\mathbf{u}}_k\|}{\|\mathbf{b}_k\|}. \quad (32)$$

Using this norm, we impose the condition, $r_{\text{rom}} < \epsilon_{\text{rom}}$, for some threshold $\epsilon_{\text{rom}} \in \mathbb{R}_+$. The threshold is defined as

$$\epsilon_{\text{rom}} := \kappa_{\text{rom}} \cdot r_{\text{kkt}}, \quad (33)$$

where the reduction factor, $0 < \kappa_{\text{rom}} < 1$, controls the tightness of the ROM accuracy and $r_{\text{kkt}} \in \mathbb{R}_+$ denotes the norm of the KKT conditions. A smaller value of κ_{rom} expects a higher accuracy of the ROM. The norm of the KKT conditions, r_{kkt} , determines how far the current point is from the optimal design point. A large value of r_{kkt} indicates that the current design variables are far from the optimal and a small value of r_{kkt} indicates the other way around. Therefore, the ROM solutions are allowed if the current design variables are far from the optimal. Otherwise, it is not allowed.

Finally, if the condition in (33) holds true, we consider that the ROM solution is good enough to be used as a solution of (11). Otherwise, we invoke the ROM-recycling Krylov subspace method to compute a better solution than the ROM solution in a fast fashion. It is described in Section 5.2.

5.2 ROM-recycling conjugate-gradient method

The system matrices arising from structural topology optimization problem, e.g., \mathbf{A}_k in Eq. (11), are usually sparse symmetric positive-definite matrices. Therefore, we consider the Conjugate Gradient (CG) method developed by Hestenes and Stiefel [34]. However, we emphasize that our ROM-recycling approach can be applied to other iterative methods, such as MINRES [50, 64] for symmetric indefinite systems and GCROT [23, 51] and GMRES [58] for more general nonsingular systems. No matter what Krylov subspace iterative linear solver is used, a preconditioner needs to be applied to reduce the number of iterations for a large-scale problem. Thus, we consider Preconditioned CG (PCG) and use Algebraic Multigrid Preconditioner (AMG) implemented in the scalable linear solver, HYPRE [5].

The PCG method solves the following minimization problem at its j th iteration:

$$\mathbf{u}_k^{(j)} = \arg \min_{\mathbf{u} \in \mathbf{u}_k^{(0)} + \mathcal{K}_k^{(j)}} \|\mathbf{u}_k^* - \mathbf{u}\|_{\mathbf{A}_k} \quad (34)$$

where $\mathbf{u}_k^{(0)}$ denotes a initial guess for the PCG process, \mathbf{u}_k^* denotes the solution for the k th linear system, $\mathcal{K}_k^{(j)} := \text{span}\{\mathbf{P}_k^{-1} \mathbf{r}_k, \mathbf{P}_k^{-1} \mathbf{A}_k \mathbf{r}_k, \dots, \mathbf{P}_k^{-1} \mathbf{A}_k^{j-1} \mathbf{r}_k\}$ denotes the Krylov subspace at the j th PCG iteration of the k th linear system solve, $\mathbf{r}_k := \mathbf{b}_k - \mathbf{A}_k \mathbf{u}_k^{(0)}$ denotes the residual vector at the k th linear system solve, $\|\mathbf{x}\|_{\mathbf{A}_k} := \sqrt{\mathbf{x}^T \mathbf{A}_k \mathbf{x}}$ denotes the \mathbf{A}_k -weighted norm, and \mathbf{P}_k^{-1} denotes a preconditioner at k th linear system solve. The solution to Problem (34) can be written as:

$$\mathbf{u}_k^{(j)} = \mathbf{u}_k^{(0)} + \mathbf{W}_k^{(j)} (\mathbf{W}_k^{(j)T} \mathbf{A}_k \mathbf{W}_k^{(j)})^{-1} \mathbf{W}_k^{(j)T} \mathbf{r}_k, \quad (35)$$

where $\mathbf{W}_k^{(j)} \in \mathbb{R}^{N_s \times j}$ denotes a basis matrix for the Krylov subspace, $\mathcal{K}_k^{(j)}$. The basis matrix, $\mathbf{W}_k^{(j)}$, satisfies \mathbf{A}_k -orthogonality, i.e., $\mathbf{W}_k^{(j)T} \mathbf{A}_k \mathbf{W}_k^{(j)} = \mathbf{\Gamma}_k^{(j)}$, where $\mathbf{\Gamma}_k^{(j)}$ is diagonal. Eq. (35) can be viewed as the Galerkin projection,

i.e., first solve for $\hat{\mathbf{u}}_k^{(j)}$ in the following reduced system:

$$\mathbf{W}_k^{(j)T} \mathbf{A}_k \mathbf{W}_k^{(j)} \hat{\mathbf{u}}_k^{(j)} = \mathbf{W}_k^{(j)T} \mathbf{r}_k, \quad (36)$$

and then set $\mathbf{u}_k^{(j)} = \mathbf{u}_k^{(0)} + \mathbf{W}_k^{(j)} \hat{\mathbf{u}}_k^{(j)}$. Note that this is identical procedure described in Eqs. (31) and (30).

The idea of recycling the Krylov subspace iterative linear solver comes from the context of solving a sequence of linear system of equations, e.g., Eq. (11). It reuses data generated from the previous linear solves to reduce the iteration number for convergence of the current linear solve. That is, the recycling PCG algorithm introduces *augmented* subspace, \mathcal{G}_k , in addition to the Krylov subspace, $\mathbf{W}_k^{(j)}$, to jump start the PCG process, i.e.,

$$\mathbf{u}_k^{(j)} = \arg \min_{\mathbf{u} \in \mathbf{u}_k^{(0)} + \mathcal{G}_k + \mathcal{K}_k^{(j)}} \|\mathbf{u}_k^* - \mathbf{u}\|_{\mathbf{A}_k}. \quad (37)$$

The augmented subspace \mathcal{G}_k is constructed, using the previous linear system solves [64, 48, 57, 27, 53]. It can be effective as long as the dimension of the subspace is not big. However, it is susceptible to the disadvantage of increasing the dimension of the augmented subspace as the number of linear system solves increases. Therefore, the truncation of the augmented subspace is needed. We accomplish the truncation, using the reduced basis, Φ_k , generated by the incremental algorithms in Section 4. By compressing previous solutions in a reduced basis in an optimal way, i.e., in the POD sense, an important subspace information from previous solutions are kept within a small dimensional subspace. In summary, we define the augmented subspace, i.e., $\mathcal{G}_k := \text{range}(\Phi_k)$. Then, the recycling PCG method generates the Krylov basis matrix, $\mathbf{W}_k^{(j)}$, that is \mathbf{A}_k -orthogonal to the augmented subspace, \mathcal{G}_k , i.e.,

$$\mathbf{W}_k^{(j)T} \mathbf{A}_k \Phi_k = \mathbf{0}, \quad \forall j \quad (38)$$

Algorithm 5 describes the ROM-recycling PCG method. For the brevity, we skip both the subscripts and superscripts of each variables. If the red blocks are omitted, then the algorithm falls into a usual PCG method. Note that the Krylov subspace basis vector, \mathbf{p} , is modified by the solution from Galerkin projection, i.e., Lines 3–4 and 26–27 of Algorithm 5. The simple subtraction of the Galerkin part from \mathbf{p} is to ensure the \mathbf{A}_k -orthogonality expressed in Eq. (38).

We set the initial guess for the ROM-recycling PCG to be the solution of the *ROM solve* in Figure 2, i.e., $\mathbf{u}^{(0)} = \tilde{\mathbf{u}}_k$ of Eq. (30). The motivation for this choice can be explained by the fact that $\tilde{\mathbf{u}}_k$ of Eq. (30) is the solution of the following minimization problem:

$$\tilde{\mathbf{u}}_k = \arg \min_{\mathbf{u} \in \mathbf{u}_k^{\text{ref}} + \mathcal{G}_k} \|\mathbf{u}_k^* - \mathbf{u}\|_{\mathbf{A}_k}. \quad (39)$$

Therefore, this choice of the initial guess makes the optimal starting point in the sense of Eq. (39).

As in the projection-based ROM of Section 5.1, we set the PCG convergence threshold, ϵ_{pcg} , relative to the value of the norm of the KKT conditions, r_{kkt} . More specifically, we provide the following two options:

1. The first one sets ϵ_{pcg} in the following way:

$$\epsilon_{\text{pcg}} := \min(\max(\kappa_{\text{pcg}} \cdot r_{\text{kkt}}, \epsilon_{\text{pcg}}^{\text{lower}}), \epsilon_{\text{pcg}}^{\text{upper}}), \quad (40)$$

where the reduction factor, $0 < \kappa_{\text{pcg}} < 1$, controls the tightness of the PCG accuracy. A smaller value of κ_{pcg} expects a higher accuracy of the PCG solution. Also, we include the norm of the KKT conditions, r_{kkt} , in the definition of ϵ_{pcg} to determine how far the current point is from the optimal design point. A large value of r_{kkt} indicates that the current design variables are far from the optimal and a small value of r_{kkt} indicates the other way around. Therefore, the less precise PCG solutions are allowed if the current design variables are far from the optimal. Otherwise, the more accurate PCG solution must be computed. Additionally, we introduce the two safeguard thresholds, $\epsilon_{\text{pcg}}^{\text{lower}}$ and $\epsilon_{\text{pcg}}^{\text{upper}}$, such as $\epsilon_{\text{pcg}}^{\text{lower}} < \epsilon_{\text{pcg}}^{\text{upper}}$. The lower bound of the PCG convergence threshold is set by $\epsilon_{\text{pcg}}^{\text{lower}}$, while $\epsilon_{\text{pcg}}^{\text{upper}}$ serves as the upper bound. This is to avoid the case when the KKT norm is either too large or too low.

2. The second choice explicitly introduces a cut value, κ_{cut} , for the PCG convergence threshold. If $r_{\text{kkt}} > \kappa_{\text{cut}}$, then we set $\epsilon_{\text{pcg}} = \max(\kappa_{\text{pcg}} \cdot r_{\text{kkt}}, \epsilon_{\text{pcg}})$. Otherwise, we set $\epsilon_{\text{pcg}} = \epsilon_{\text{pcg}}$. This implies that if the norm of the KKT conditions is greater than the cut value, then we allow the inexact solve by the PCG because the current point is far away from an optimal point and the linear solve does not need to be solved precisely. If $r_{\text{kkt}} \leq \kappa_{\text{cut}}$, we set the PCG convergence threshold to be a user-defined threshold, i.e., ϵ_{pcg} . Therefore, the minimum threshold this option can take is ϵ_{pcg} .

6 Numerical experiments

We provide numerical evidences of the advantages of our method in several numerical experiments with structural topology optimization. We consider two different types of topology optimization problems: 1) compliance minimization problem with mass constraint and 2) the mass minimization problems with stress constraint.

For all the numerical examples considered herein, we use the second option of setting ϵ_{pcg} described in Section 5.2. All the simulations use a number of processors in Quartz of Livermore Computing Center⁶. All the visualizations are made with VisIt⁷. The default and our ROM-based topology optimization methods are compared. The default method follows the flow chart in Figure 1a where *physics PDE solve* and *sensitivity analysis* are solved by PCG without ROM-recycling, i.e., see Algorithm 5 without red blocks, but with AMG preconditioner from HYPRE. Zero initial guess is used in the PCG iterations and we set $\epsilon_{\text{pcg}} = \epsilon_{\text{pcg}}$ for the default method. For the ROM-based topology optimization methods, we consider both incremental QR (see Algorithms 1 and 2) and SVD (see Algorithms 3 and 4) to construct reduced bases. Both incremental algorithms are implemented in an open source library, libROM [19].

6.1 Compliance minimization

Two 3D design problems are considered: i) cantilever beam, and ii) wind turbine blade.

6.1.1 3D cantilever beam design

Cantilever beam design problem is the same as the numerical examples considered in [64]. The design domains and optimal designs for two problems are shown in Figure 3. Compliance minimization with total mass constraint is considered. Three different mesh resolutions are considered: 3 000, 24 000, and 192 000 design variables. The following material properties are used: Young’s modulus of $2.0 \times 10^{11} \text{ N/m}^2$ and Poisson’s ratio of 0.29. The upper bound for the mass constraint is 0.5 and the SIMP parameter is $s = 3$ in Eq. (4). IPOPT is used as an optimization solver with convergence threshold of 10^{-6} . We use the Helmholtz filter with $r = 0.1 \text{ m}$. Finally, the following ROM-based topology optimization parameters are used: $\kappa_{\text{rom}} = \kappa_{\text{pcg}} = 10^{-2}$, $\kappa_{\text{cut}} = 10^{-3}$, $\epsilon_{\text{pcg}} = 10^{-4}$, $\epsilon_{\text{QR}} = \epsilon_{\text{SVD}} = 10^{-9}$, and $r_{\text{max}} = 10$. All the simulations for the cantilever beam design problem use 36 processors in Quartz. A structured mesh with uniform hexahedral first-order finite elements is used for the discretization.

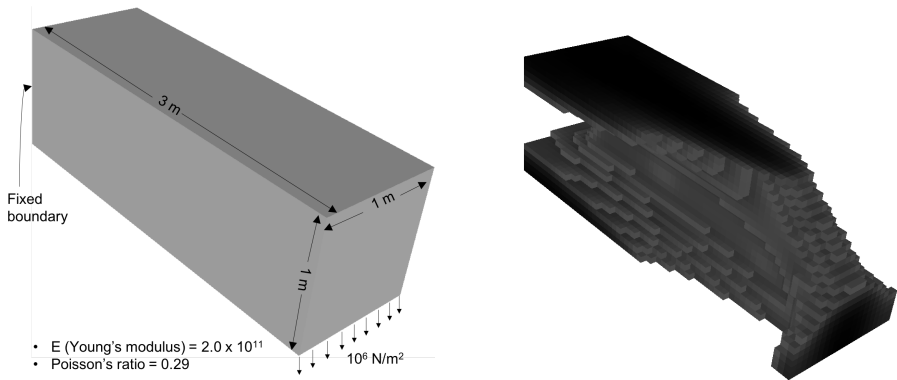


Figure 3: Left: design domain, Right: an optimal design for the cantilever beam

Tables 1, 2, and 3 show the performance comparison among the default and ROM-based topology optimization methods with incremental QR and SVD for the 3D cantilever beam design problems with different number of design variables. They have the comparable optimal compliance values although ROM-based approach with incremental SVD gives slightly worse optimal value with 3,000 design variables in Table 1. It converges to a different local minimum. The ROM-based approach with incremental SVD converges within 113 IPOPT iterations, while the other approaches take around 300 iterations. Therefore, it results in a tremendous reduction in total number of iterations in linear solve, i.e., 15.4 as well as a considerable speed-up for the solving time, i.e., 4.1.

Other cases with more design variables, i.e., Tables 2 and 3, all the methods converge to the same design with the same optimal compliance value. In terms of the total wall clock time of linear solves, the ROM-based approach achieves a considerable speed-up of 2.2 to 3.5. The average number of iterations in linear solves are also reduced

⁶<https://hpc.llnl.gov/hardware/platforms/Quartz>

⁷<https://wci.llnl.gov/simulation/computer-codes/visit>

	Default	ROM-based top.opt. incremental QR	ROM-based top.opt. incremental SVD
Optimal compliance	13.59	13.59	13.63
Total wall clock time of linear solve (sec.)	41.9	26.2	10.2
Total iters. of linear solve	7,700	1,528	500
Avg. iters. of linear solve	23.5	5.2	4.3
IPOPT iter.	297	294	113
KKT norm	6.68e-7	4.86e-7	6.56e-7
Speed-up of total linear solve	1.0	1.6	4.1
Avg. iter. reduction of linear solve	1.0	2.4	5.5
Total iter. reduction of linear solve	1.0	5.0	15.4

Table 1: performance comparison for cantilever beam 3D design problem with 3,000 design variables.

	Default	ROM-based top.opt. incremental QR	ROM-based top.opt. incremental SVD
Optimal compliance	13.2	13.2	13.2
Total wall clock time of linear solve (sec.)	241.2	108.4	69.8
Total iters. of linear solve	6,789	1,083	799
Avg. iters. of linear solve	24.2	6.4	7.3
IPOPT iter.	180	168	108
KKT norm	7.74e-7	6.73e-7	8.11e-7
Speed-up of total linear solve	1.0	2.2	3.5
Avg. iter. reduction of linear solve	1.0	3.8	3.3
Total iter. reduction of linear solve	1.0	6.3	8.5

Table 2: performance comparison for cantilever beam 3D design problem with 24,000 design variables.

considerably by a factor of up to 3.1 to 3.8. For these particular problems, the ROM-based approaches converge to optimal solutions with less number of IPOPT iterations than the default method. Therefore, the reduction factor of the total number linear solve iterations is quite big, i.e., from 3.3 to 8.5.

6.1.2 Wind turbine blade design

To obtain an optimal blade design problem, we consider minimizing compliance with a total mass constraint. The design domain is described in Figure 4. A fixed boundary condition is applied to the thicker end of the blade. The blade problem has 414,979 design variables. In order to mimic wind conditions, two load cases are considered: 10 N in x -direction and 10 N in y -direction. Two different compliance values are computed for two different loads, then the average compliance is minimized. The following material properties are used: Young’s modulus of 2.0×10^{11} N/m^2 and Poisson’s ratio of 0.29. The upper bound for the mass constraint is 0.25. The SIMP parameter $s = 3$ is used in Eq. (4). IPOPT is used as an optimization solver with convergence threshold of 10^{-6} . The mass matrix filter described in Section 2 is used to avoid checkerboard problem. Finally, the following ROM-based topology optimization parameters are used: $\kappa_{\text{rom}} = \kappa_{\text{pcg}} = 10^{-3}$, $\kappa_{\text{cut}} = 10^{-3}$, $\varepsilon_{\text{pcg}} = 10^{-4}$, $\epsilon_{\text{QR}} = \epsilon_{\text{SVD}} = 10^{-9}$, and $r_{\text{max}} = 10$. All the simulations for the blade design problem use 72 processors from Quartz.

One difference between the blade problem and the 3D cantilever beam problem in the previous section is mesh. An unstructured mesh with tetrahedral first-order finite elements is used for the discretization of the blade. Because of the unstructured mesh, the default method with AMG preconditioner from HYPRE is not enough to bring down the number of PCG iterations as shown in Table 4, i.e., 265.5 average number of iterations per a linear solve is required for the default method. On the other hand, the ROM-based approaches take only 25.8 and 27.3 average number of iterations for incremental QR and SVD, respectively. This gives the reduction factor of around 10. Our method also achieves considerable speed-ups in terms of linear system solving times, i.e., larger than 3, reducing total wall-clock time from 1.7 hours to 0.55 or 0.48 hours, even though our ROM-based approaches take more IPOPT iterations than the default method. Note that the three different methods produce the identical optimal compliance value, i.e., 2.61. These optimal designs satisfy the KKT optimality conditions, implying that the quality of the design

	Default	ROM-based top.opt. incremental QR	ROM-based top.opt. incremental SVD
Optimal compliance	13.6	13.6	13.6
Total wall clock time of linear solve (sec.)	761.8	267.5	238.3
Total iters. of linear solve	3,229	942	989
Avg. iters. of linear solve	24.1	6.5	7.9
IPOPT iter.	132	142	123
KKT norm	9.5-e-7	8.07e-7	9.86e-7
Speed-up of total linear solve	1.0	2.8	3.2
Avg. iter. reduction of linear solve	1.0	3.7	3.1
Total iter. reduction of linear solve	1.0	3.4	3.3

Table 3: performance comparison for cantilever beam 3D design problems with 192,000 design variables.

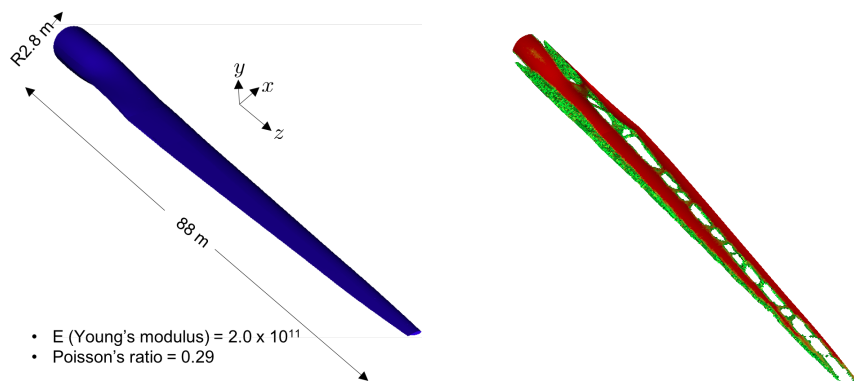


Figure 4: Left: design domain, Right: an optimal design for the wind turbine blade

is not degraded by the approximation introduced by the ROMs.

6.2 Stress-constrained problem

Our method can be applicable not only to the compliance minimization problems, but also to stress-constrained design problems. We demonstrate it in this section by considering a classical stress constrained topology optimization problem, i.e., L-bracket problem.

6.2.1 L-bracket problem

A classical L-bracket stress-constrained problem is considered. The design domain, boundary conditions, and external loading are described in Figure 5. The total mass is minimized with a stress constraint. The von Mises stress criterion is used as a stress quantity and p-norm with $p = 8$ is used to approximate the maximum stress value as in [43]. The following material properties are used: Young's modulus of $10^6 N/m^2$ and Poisson's ratio of 0.3. The number of design variables is 102,400. The upper bound for the stress constraint is $20N/m^2$ and the SIMP parameter is $s = 3$ in Eq. (4). Stress quantity penalization parameter $q = 0.5$ in Eq. (5) is used. The Helmholtz filter with $r = 0.0005 m$ is used. IPOPT is used as an optimization solver with convergence threshold of 10^{-6} . Finally, we use the following ROM-based topology optimization parameters: $\kappa_{rom} = \kappa_{pcg} = 10^{-3}$, $\kappa_{cut} = 10^{-3}$, $\epsilon_{pcg} = 10^{-4}$, $\epsilon_{QR} = \epsilon_{SVD} = 10^{-9}$, and $r_{max} = 10$. All the simulations for the stress-constrained problems use 144 processors in Quartz.

A structured mesh with uniform quadrilateral first-order finite elements is used for the discretization. Therefore, the default method with AMG preconditioner is able to reduce the number of linear solve iteration sufficiently. However, we still see a further reduction and speed-up by applying our ROM-based approach. For example, the default method requires 61.0 iterations in average per a linear solve, while the ROM-based approaches with incremental QR and SVD require 39.5 and 46.5 iterations, respectively. This gives reduction of 1.5 and 1.3, respectively. The wall clock time for the default method is 1.5 hours, while the ROM-based approaches finish within 0.71 hours, resulting

	Default	ROM-based top.opt. incremental QR	ROM-based top.opt. incremental SVD
Optimal compliance	2.61	2.61	2.61
Total wall clock time of linear solve (hour)	1.70	0.55	0.48
Total iters. of linear solve	372,196	56,542	51,062
Avg. iters. of linear solve	265.5	25.8	27.3
IPOPT iter.	664	1092	934
KKT norm	9.82e-7	8.71e-7	7.47e-7
Speed-up of total linear solve	1.0	3.1	3.5
Avg. iter. reduction of linear solve	1.0	10.3	9.5
Total iter. reduction of linear solve	1.0	6.6	9.7

Table 4: performance comparison for wind turbine blade 3D design problem.

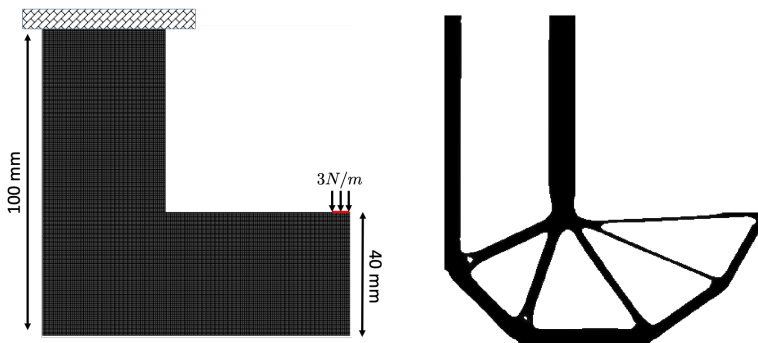


Figure 5: L-bracket stress-constrained problem, Left: design domain, boundary conditions, and external load, Right: an optimal design

in a speed-up of 2.1. Note that all the three methods produce the same optimal mass, which is 0.38. Also note that all the three methods converge to a point that satisfies the necessary optimality conditions, i.e., the KKT norms are less than $1.0e - 6$.

7 Conclusion

A ROM-based design optimization acceleration method is introduced. The overall design optimization is accelerated by accelerating linear system solves as demonstrated in Section 6. The ROM-based approach shows a considerable speed-up especially when the unstructured mesh is used, in which the default method with a AMG preconditioner requires many Krylov subspace iterations. The method is not tailored for the compliance minimization problems. It is applicable to a stress-constrained optimization problem, which is also demonstrated in numerical experiments. Furthermore, our method is general enough to be applicable to other PDE-constrained optimization problems, such as shape optimization and inverse problems. Finally, the method does not suffer from the approximation introduced by the ROM because the accuracy of ROM is carefully monitored and treated throughout the optimization process, resulting in an optimal design that satisfies the KKT optimality condition.

Future research is required to further understand the precise conditions for the inexactness. We have only provided the heuristic explanations on why our ROM-based approach works well and determines the parameter values of our method heuristically. Thorough theoretical study on the convergence rate of the interior-point method affected by the inexactness introduced by ROMs is necessary because the majority of literatures on this topic considers the inexactness coming from the optimization linear solves, not from the PDE solves. Finally, constructing reduced order operator can be computationally expensive. In reduced order model research community, a hyper-reduction is used to reduce the cost of constructing reduced order operators. This will be investigated in future to further accelerate the optimization process.

	Default	ROM-based top.opt. incremental QR	ROM-based top.opt. incremental SVD
Optimal mass	0.38	0.38	0.38
Total wall clock time of linear solve (hour)	1.5	0.7	0.71
Total iters. of linear solve	721,223	290,245	325,418
Avg. iters. of linear solve	61.0	39.5	46.5
IPOPT iter.	4,788	3,670	3,494
KKT norm	7.78e-7	6.00e-7	9.83e-7
Speed-up of total linear solve	1.0	2.1	2.1
Avg. iter. reduction of linear solve	1.0	1.5	1.3
Total iter. reduction of linear solve	1.0	2.5	2.2

Table 5: performance comparison for L-bracket stress-constrained problem.

Acknowledgments

This work was performed at Lawrence Livermore National Laboratory and was supported by the LDRD program (17-SI-005). Lawrence Livermore National Laboratory is operated by Lawrence Livermore National Security, LLC, for the U.S. Department of Energy, National Nuclear Security Administration under Contract DE-AC52-07NA27344 and LLNL-JRNL-791183.

References

- [1] G Allaire and GA Francfort. A numerical algorithm for topology and shape optimization. In *Topology design of structures*, pages 239–248. Springer, 1993.
- [2] G Allaire and RV Kohn. Topology optimization and optimal shape design using homogenization. In *Topology design of structures*, pages 207–218. Springer, 1993.
- [3] Oded Amir, Mathias Stolpe, and Ole Sigmund. Efficient use of iterative solvers in nested topology optimization. *Structural and Multidisciplinary Optimization*, 42(1):55–72, 2010.
- [4] Erik Andreassen, Anders Clausen, Mattias Schevenels, Boyan S Lazarov, and Ole Sigmund. Efficient topology optimization in matlab using 88 lines of code. *Structural and Multidisciplinary Optimization*, 43(1):1–16, 2011.
- [5] Allison H Baker, Robert D Falgout, Tzanio V Kolev, and Ulrike Meier Yang. Scaling hypres multigrid solvers to 100,000 cores. In *High-Performance Scientific Computing*, pages 261–279. Springer, 2012.
- [6] Andrew T Barker, Tyrone Rees, and Martin Stoll. A fast solver for an \mathcal{H}_1 regularized PDE-constrained optimization problem. *Communications in Computational Physics*, 19(01):143–167, 2016.
- [7] Stefania Bellavia. Inexact interior-point method. *Journal of Optimization Theory and Applications*, 96(1):109–121, 1998.
- [8] Martin P Bendsøe. Optimal shape design as a material distribution problem. *Structural optimization*, 1(4):193–202, 1989.
- [9] Martin P Bendsøe and Ole Sigmund. Material interpolation schemes in topology optimization. *Archive of applied mechanics*, 69(9-10):635–654, 1999.
- [10] Gal Berkooz, Philip Holmes, and John L Lumley. The proper orthogonal decomposition in the analysis of turbulent flows. *Annual review of fluid mechanics*, 25(1):539–575, 1993.
- [11] Paul T Boggs and Jon W Tolle. Sequential quadratic programming. *Acta numerica*, 4:1–51, 1995.
- [12] Blaise Bourdin. Filters in topology optimization. *International journal for numerical methods in engineering*, 50(9):2143–2158, 2001.
- [13] Matthew Brand. Incremental singular value decomposition of uncertain data with missing values. In *European Conference on Computer Vision*, pages 707–720. Springer, 2002.
- [14] Tyler E Bruns and Daniel A Tortorelli. Topology optimization of non-linear elastic structures and compliant mechanisms. *Computer methods in applied mechanics and engineering*, 190(26-27):3443–3459, 2001.

- [15] Richard H Byrd, Frank E Curtis, and Jorge Nocedal. An inexact sqp method for equality constrained optimization. *SIAM Journal on Optimization*, 19(1):351–369, 2008.
- [16] Richard H Byrd, Jean Charles Gilbert, and Jorge Nocedal. A trust region method based on interior point techniques for nonlinear programming. *Mathematical programming*, 89(1):149–185, 2000.
- [17] Kevin Carlberg, Virginia Forstall, and Ray Tuminaro. Krylov-subspace recycling via the pod-augmented conjugate-gradient method. *SIAM Journal on Matrix Analysis and Applications*, 37(3):1304–1336, 2016.
- [18] Saifon Chaturantabut and Danny C Sorensen. Nonlinear model reduction via discrete empirical interpolation. *SIAM Journal on Scientific Computing*, 32(5):2737–2764, 2010.
- [19] Youngsoo Choi, William J. Arrighi, Dylan M. Copeland, Robert W. Anderson, Geoffrey M. Oxberry, and USDOE National Nuclear Security Administration. librom, 10 2019.
- [20] Youngsoo Choi, Deshawn Coombs, and Robert Anderson. SNS: A solution-based nonlinear subspace method for time-dependent nonlinear model order reduction. *arXiv preprint arXiv:1809.04064*, 2018.
- [21] Youngsoo Choi, Charbel Farhat, Walter Murray, and Michael Saunders. A practical factorization of a Schur complement for PDE-constrained distributed optimal control. *Journal of Scientific Computing*, 65(2):576–597, 2015.
- [22] Andrew R Conn, GIM Gould, and Philippe L Toint. *LANCELOT: a Fortran package for large-scale nonlinear optimization (Release A)*, volume 17. Springer Science & Business Media, 2013.
- [23] Eric De Sturler. Truncation strategies for optimal krylov subspace methods. *SIAM Journal on Numerical Analysis*, 36(3):864–889, 1999.
- [24] Joshua D Deaton and Ramana V Grandhi. A survey of structural and multidisciplinary continuum topology optimization: post 2000. *Structural and Multidisciplinary Optimization*, 49(1):1–38, 2014.
- [25] Alejandro Diaz and Ole Sigmund. Checkerboard patterns in layout optimization. *Structural optimization*, 10(1):40–45, 1995.
- [26] Zlatko Drmac and Serkan Gugercin. A new selection operator for the discrete empirical interpolation method—improved a priori error bound and extensions. *SIAM Journal on Scientific Computing*, 38(2):A631–A648, 2016.
- [27] Jocelyne Erhel and Frédéric Guyomarc’h. An augmented conjugate gradient method for solving consecutive symmetric positive definite linear systems. *SIAM Journal on Matrix Analysis and Applications*, 21(4):1279–1299, 2000.
- [28] Claude Fleury. Conlin: an efficient dual optimizer based on convex approximation concepts. *Structural optimization*, 1(2):81–89, 1989.
- [29] Anders Forsgren and Philip E Gill. Primal-dual interior methods for nonconvex nonlinear programming. *SIAM Journal on Optimization*, 8(4):1132–1152, 1998.
- [30] Anders Forsgren, Philip E Gill, and Margaret H Wright. Interior methods for nonlinear optimization. *SIAM review*, 44(4):525–597, 2002.
- [31] Christian Gogu. Improving the efficiency of large scale topology optimization through on-the-fly reduced order model construction. *International Journal for Numerical Methods in Engineering*, 101(4):281–304, 2015.
- [32] Gene Golub and Charles F. Van Loan. *Matrix Computations (3rd ed.)*. Johns Hopkins, 1996.
- [33] Matthias Heinkenschloss and Luis N Vicente. Analysis of inexact trust-region sqp algorithms. *SIAM Journal on Optimization*, 12(2):283–302, 2002.
- [34] Magnus Rudolph Hestenes and Eduard Stiefel. *Methods of conjugate gradients for solving linear systems*, volume 49. 1952.
- [35] Michael Hinze and Stefan Volkwein. Proper orthogonal decomposition surrogate models for nonlinear dynamical systems: Error estimates and suboptimal control. In *Dimension reduction of large-scale systems*, pages 261–306. Springer, 2005.
- [36] Harold Hotelling. Analysis of a complex of statistical variables into principal components. *Journal of educational psychology*, 24(6):417, 1933.
- [37] Thomas JR Hughes. *The finite element method: linear static and dynamic finite element analysis*. Courier Corporation, 2012.
- [38] Chandrashekhar S Jog and Robert B Haber. Stability of finite element models for distributed-parameter optimization and topology design. *Computer methods in applied mechanics and engineering*, 130(3-4):203–226, 1996.

- [39] Zhan Kang, Chi Zhang, and Gengdong Cheng. Structural topology optimization considering mass moment of inertia.
- [40] Atsushi Kawamoto, Tadayoshi Matsumori, Shintaro Yamasaki, Tsuyoshi Nomura, Tsuguo Kondoh, and Shinji Nishiwaki. Heaviside projection based topology optimization by a pde-filtered scalar function. *Structural and Multidisciplinary Optimization*, 44(1):19–24, 2011.
- [41] Karl Kunisch and Stefan Volkwein. Galerkin proper orthogonal decomposition methods for a general equation in fluid dynamics. *SIAM Journal on Numerical analysis*, 40(2):492–515, 2002.
- [42] Boyan Stefanov Lazarov and Ole Sigmund. Filters in topology optimization based on helmholtz-type differential equations. *International Journal for Numerical Methods in Engineering*, 86(6):765–781, 2011.
- [43] Chau Le, Julian Norato, Tyler Bruns, Christopher Ha, and Daniel Tortorelli. Stress-based topology optimization for continua. *Structural and Multidisciplinary Optimization*, 41(4):605–620, 2010.
- [44] Michel Loeve. *Probability Theory*. D. Van Nostrand, New York, 1955.
- [45] Yangjun Luo and Zhan Kang. Topology optimization of continuum structures with drucker–prager yield stress constraints. *Computers & Structures*, 90:65–75, 2012.
- [46] HP Mlejnek. Some aspects of the genesis of structures. *Structural optimization*, 5(1-2):64–69, 1992.
- [47] Ngoc-Cuong Nguyen and Yanlai Chen. Reduced-basis method for the iterative solution of parametrized symmetric positive-definite linear systems. *arXiv preprint arXiv:1804.06363*, 2018.
- [48] Dianne P O’Leary. The block conjugate gradient algorithm and related methods. *Linear algebra and its applications*, 29:293–322, 1980.
- [49] Geoffrey M Oxberry, Tanya Kostova-Vassilevska, William Arrighi, and Kyle Chand. Limited-memory adaptive snapshot selection for proper orthogonal decomposition. *International Journal for Numerical Methods in Engineering*, 109(2):198–217, 2017.
- [50] Christopher C Paige and Michael A Saunders. Solution of sparse indefinite systems of linear equations. *SIAM journal on numerical analysis*, 12(4):617–629, 1975.
- [51] Michael L Parks, Eric De Sturler, Greg Mackey, Duane D Johnson, and Spandan Maiti. Recycling krylov subspaces for sequences of linear systems. *SIAM Journal on Scientific Computing*, 28(5):1651–1674, 2006.
- [52] Tyrone Rees, Martin Stoll, and Andy Wathen. All-at-once preconditioning in PDE-constrained optimization. *Kybernetika*, 46(2):341–360, 2010.
- [53] Franck Risler and Christian Rey. Iterative accelerating algorithms with krylov subspaces for the solution to large-scale nonlinear problems. *Numerical algorithms*, 23(1):1, 2000.
- [54] Susana Rojas-Labanda and Mathias Stolpe. Benchmarking optimization solvers for structural topology optimization. *Structural and Multidisciplinary Optimization*, 52(3):527–547, 2015.
- [55] George IN Rozvany. *Structural design via optimality criteria: the Prager approach to structural optimization*. Kluwer Academic Publisher & Dordrecht, 1989.
- [56] GIN Rozvany and Ming Zhou. The coc algorithm, part i: cross-section optimization or sizing. *Computer Methods in Applied Mechanics and Engineering*, 89(1-3):281–308, 1991.
- [57] Youcef Saad. On the lanczos method for solving symmetric linear systems with several right-hand sides. *Mathematics of computation*, 48(178):651–662, 1987.
- [58] Yousef Saad. Analysis of augmented krylov subspace methods. *SIAM Journal on Matrix Analysis and Applications*, 18(2):435–449, 1997.
- [59] Ole Sigmund and Kurt Maute. Topology optimization approaches. *Structural and Multidisciplinary Optimization*, 48(6):1031–1055, 2013.
- [60] Ole Sigmund and Joakim Petersson. Numerical instabilities in topology optimization: a survey on procedures dealing with checkerboards, mesh-dependencies and local minima. *Structural optimization*, 16(1):68–75, 1998.
- [61] Mathias Stolpe and Krister Svanberg. An alternative interpolation scheme for minimum compliance topology optimization. *Structural and Multidisciplinary Optimization*, 22(2):116–124, 2001.
- [62] Krister Svanberg. The method of moving asymptotes a new method for structural optimization. *International journal for numerical methods in engineering*, 24(2):359–373, 1987.
- [63] Andreas Wächter and Lorenz T Biegler. On the implementation of an interior-point filter line-search algorithm for large-scale nonlinear programming. *Mathematical programming*, 106(1):25–57, 2006.

- [64] Shun Wang, Eric de Sturler, and Glaucio H Paulino. Large-scale topology optimization using preconditioned krylov subspace methods with recycling. *International journal for numerical methods in engineering*, 69(12):2441–2468, 2007.
- [65] Gil Ho Yoon. Structural topology optimization for frequency response problem using model reduction schemes. *Computer Methods in Applied Mechanics and Engineering*, 199(25-28):1744–1763, 2010.
- [66] M Zhou and GIN Rozvany. The coc algorithm, part ii: Topological, geometrical and generalized shape optimization. *Computer Methods in Applied Mechanics and Engineering*, 89(1-3):309–336, 1991.

Algorithm 5 ROM-recycling PCG

(YC: Redefine the notation here)

$\mathbf{u} = \mathbf{ROMrecyclingPCG}(\mathbf{A}, \mathbf{b}, \mathbf{u}^{(0)}, \epsilon_{\text{pcg}}, \epsilon_{\text{abs}}, N_{\text{maxit}}, \mathbf{P}^{-1}, \Phi)$

Input: $\mathbf{A}, \mathbf{b}, \mathbf{u}, \epsilon_{\text{pcg}}, \epsilon_{\text{abs}}, N_{\text{maxit}}, \mathbf{P}^{-1}, \Phi$

Output: \mathbf{u}

```
1:  $\mathbf{r} \leftarrow \mathbf{b} - \mathbf{A}\mathbf{u}^{(0)}$ 
2:  $\mathbf{p} \leftarrow \mathbf{P}^{-1}\mathbf{r}$ 
3: solve  $\Phi^T \mathbf{A} \Phi \hat{\mathbf{u}} = \Phi^T \mathbf{A} \mathbf{p}$ 
4:  $\mathbf{p} \leftarrow \mathbf{p} - \Phi \hat{\mathbf{u}}$ 
5:  $r_0 \leftarrow \max(\epsilon_{\text{pcg}}^2 \mathbf{b}^T \mathbf{P}^{-1} \mathbf{b}, \epsilon_{\text{abs}}^2)$ 
6:  $\zeta \leftarrow \mathbf{r}^T \mathbf{p}$ 
7: if  $\zeta \leq r_0$  then
8:   converged
9: end if
10:  $\mathbf{z} \leftarrow \mathbf{A} \mathbf{p}$ 
11:  $\gamma \leftarrow \mathbf{z}^T \mathbf{p}$ 
12: if  $\gamma = 0$  then
13:   fail to converge
14: end if
15: for  $j = 1, \dots, N_{\text{maxit}}$  do
16:    $\alpha \leftarrow \frac{\zeta}{\gamma}$ 
17:    $\mathbf{u} \leftarrow \mathbf{u} + \alpha \mathbf{p}$ 
18:    $\mathbf{r} \leftarrow \mathbf{r} - \alpha \mathbf{A} \mathbf{p}$ 
19:    $\mathbf{z} \leftarrow \mathbf{P}^{-1} \mathbf{r}$ 
20:    $\eta \leftarrow \mathbf{r}^T \mathbf{z}$ 
21:   if  $\eta < r_0$  then
22:     converged
23:   end if
24:    $\beta \leftarrow \frac{\eta}{\zeta}$ 
25:    $\mathbf{p} \leftarrow \mathbf{z} + \beta \mathbf{p}$ 
26:   solve  $\Phi^T \mathbf{A} \Phi \hat{\mathbf{u}} = \Phi^T \mathbf{A} \mathbf{z}$ 
27:    $\mathbf{p} \leftarrow \mathbf{p} - \Phi \hat{\mathbf{u}}$ 
28:    $\mathbf{z} \leftarrow \mathbf{A} \mathbf{p}$ 
29:    $\gamma \leftarrow \mathbf{p}^T \mathbf{z}$ 
30:   if  $\gamma \leq 0$  then
31:     not positive definite
32:   end if
33:    $\zeta \leftarrow \eta$ 
34: end for
```
